QUEST Technical Report No. 541

EMBEDDED OPTICAL FIBER ICE STRESS GAUGE
PHASE I FINAL REPORT

J. J. Kollé

October 1991

Prepared for
OFFICE OF NAVAL RESEARCH
Under Contract No. N00014-91-C-0075

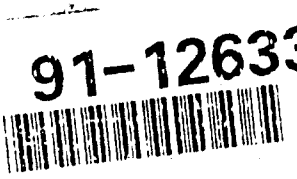

QUEST Integrated, Inc.
21414 - 68th Avenue South
Kent, Washington 98032
(206) 872-9500

REPORT DOCUMENTATION PAGE

Form Approved
OMB No 0704 0188

1. AGENCY USE ONLY (Leave blank)	2. REPORT DATE	3. REPORT TYPE AND DATES COVERED
	October 1991	Final Report 3/1/91 - 8/31/91

4. TITLE AND SUBTITLE
Embedded Optical Fiber Stress Gauge

5. FUNDING NUMBERS
N00014-91-C-0075

6. AUTHOR(S)
J.J. Kolle

7. PERFORMING ORGANIZATION NAME(S) AND ADDRESS(ES)
QUEST Integrated, Inc.
21414 - 68th Avenue South
Kent, Washington 98032

8. PERFORMING ORGANIZATION REPORT NUMBER
Technical Report 541

9. SPONSORING/MONITORING AGENCY NAME(S) AND ADDRESS(ES)
DCMAO Seattle
Bldg. 5D Naval Station Puget Sound
Seattle, Washington 98115-5010

10. SPONSORING/MONITORING AGENCY REPORT NUMBER

11. SUPPLEMENTARY NOTES

12a. DISTRIBUTION/AVAILABILITY STATEMENT
Unlimited

12b. DISTRIBUTION CODE

13. ABSTRACT *(Max..num 200 words)*

Direct observations of ice stress provide an important constraint on models of the behavior of the Arctic ice cover. Present means of observing these stresses have been limited by gauge sensitivity, bandwidth, thermal response, and nonlinear ice behavior. This report describes a Phase I feasibility study of a new type of ice stress gauge based on an optical fiber embedded in a flat panel. The sensing mechanism used in this gauge is stress-induced birefringence, which causes a linear phase change in polarized light in the optical fiber. Tests of a prototype gauge embedded in a block of ice showed that the gauge has the sensitivity and range required for observations of sea-ice stress. The thermal sensitivity and drift characteristics of the gauge were also shown to be small. A design for a compact, low-power gauge with a diode laser light source and integrated opto-electronic polarization analyzer is also provided. This gauge would be suitable for remote field observations of the state of biaxial stress in the Arctic ice pack at a cost that is comparable to existing gauge technology.

14. SUBJECT TERMS	15. NUMBER OF PAGES
sea, ice, stress, gauge, optical, fiber, polarization birefringence	41
	16. PRICE CODE

17. SECURITY CLASSIFICATION OF REPORT	18 SECURITY CLASSIFICATION OF THIS PAGE	19 SECURITY CLASSIFICATION OF ABSTRACT	20. LIMITATION OF ABSTRACT
Unclassified	Unclassified	Unclassified	SAR

TABLE OF CONTENTS

LIST OF FIGURES AND TABLES

INTRODUCTION

Direct observations of ice stress provide an important constraint on models of the behavior of the Arctic ice cover. Present means of observing these stresses have been limited by gauge sensitivity, bandwidth, thermal response, and nonlinear ice behavior. This report describes a Phase I SBIR study conducted by QUEST Integrated, Inc., for the Office of Naval Research (ONR) to evaluate the feasibility of a new type of ice stress gauge based on an embedded optical fiber (EOF). The sensing mechanism used in the EOF gauge is stress-induced birefringence in the optical fiber. The Phase I study demonstrated the feasibility of this approach by carrying out ice stress observations with the required range and sensitivity.

The Phase I study began with a review of existing ice stress measurement techniques as well as a review of measurement techniques based on optical fiber technology. A design for a flat panel EOF gauge, based on measurement of stress-induced birefringence, was then developed. The gauge consists of an optical fiber embedded in a flat panel of cast polymer. Polarized light is launched into the fiber and analyzed after passing through the panel. Stress-induced birefringence causes the output polarization phase angle to change linearly.

A series of tests was carried out on an optical bench to verify the measurement concept and to screen materials for the gauge panel. A full-scale prototype panel was then fabricated and embedded in a block of ice. A macroscopic optical system was used to provide polarized light excitation and phase retardation analysis for tests of normal sensitivity, transverse sensitivity, and drift. The EOF gauge thermal response was also observed.

The final task in this Phase I study involved an evaluation of the design of an integrated optical system to provide gauge excitation and polarization phase analysis. The integrated EOF gauge would provide enhanced performance at a comparable cost to existing gauge technology and would be suitable for remote field observations of the state of biaxial stress in the Arctic ice pack.

This report details the work that was conducted and presents the Phase I results. The information is presented in the same order as discussed in this Introduction. Conclusions are summarized in the final section.

ICE STRESS GAUGE REVIEW

Sea ice deformation tends to be localized in small regions of high stress concentration where floe interactions such as ridging, rafting, and lead formation occur. Observations of sea ice stress indicate that peak stress levels are generally on the order of 100 kPa (Lau and Knoke, 1991), which is an order of magnitude less than the compressive strength of the sea ice. Useful observations of the stresses associated with geophysical forcing and floe interactions require a gauge with a sensitivity on the order of 1 kPa (0.1 psi) and a range of a few hundred kilopascals. The gauge should be suitable for observations of biaxial stress in both tension and compression.

The gauge should be capable of long-term measurements of signals that vary over time scales of days to months, as well as measurements of dynamic events occurring over periods of seconds to hours. The physical scale of the gauge should be small enough to allow for measurements of the variation in stress through an ice floe but still be larger than the scale of individual ice crystals. The gauge should be relatively insensitive to transverse stress and temperature variations between -40° and 0°C.

An extensive review of gauges for ice stress measurement has been provided by Cox and Johnson (1983). Ice stress gauges can be classified into two groups, rigid cylindrical inclusion gauges and flat panel gauges. In the following sections, the stress sensitivity, range, and thermal sensitivity of each type of gauge are discussed.

Rigid Cylindrical Inclusion Gauge

The most successful cylindrical inclusion gauge is the one developed by Cox and Johnson and presently marketed by the Geokon Company. The operation of this gauge relies on the fact that if the gauge stiffness is significantly higher than the stiffness of the ice in which it is embedded, then the stresses and strains in the gauge will be a constant multiple of the far-field ice stress.

The Geokon gauge uses vibrating wire technology to observe deformations in a rigid cylinder to derive the biaxial far-field ice stress. The gauge is limited to about 14 kPa (2 psi) because of the extremely small deformations that result from the high gauge stiffness. At the sensitivity limit, the vibrating wires measure displacements of about 20 nm. This resolution level could be improved using an optical interferometer, however, the complexity and cost of such a system would be much higher than the vibrating wire technique.

The Geokon gauge is sensitive to temperature variations with a response of around 5 kPa/°C change in temperature when immersed in a glycol bath.

The coefficient of thermal expansion (CTE) of ice is about 5×10^{-5}/°C compared to only 1.7×10^{-5} for steel. As the ice cools it contracts more than the steel, and a net stress is introduced in the gauge. For a rigid

gauge the inclusion stress will be equal to the stress required to expand the ice at the gauge radius by an amount determined by the CTE mismatch:

$$\sigma_T = E_i/(1+\nu)\, dr/r \tag{1}$$

where

$$dr/r = (CTE_S - CTE_i)\, dT \tag{2}$$

For typical sea ice with a modulus of 1 MPa, this effect introduces a stress of 25 kPa/°C. In multiyear ice with a modulus of 7 GPa, the error will be proportionally higher.

This result is in contrast to the experimental results of Cox and Johnson who report differential thermal expansion stresses of less than 20 kPa for a temperature excursion from -20°C to 0°C and back to -10°C. Under these conditions they conclude that rapid creep in the ice is sufficient to relax any local differential thermal expansion stress. Creep strain in polycrystalline ice at low stress levels may be described by a power law equation (Hobbs, 1974) as follows:

$$d\varepsilon/dt = C\, \tau^3 \tag{3}$$

where

$$C = A \exp(-E/kT) \tag{4}$$

and τ is shear stress, $A = 2.3 \times 10^{-9}$ Pa^{-3} s^{-1} is a constant, $E = 1.3 \times 10^{-19}$ J is the activation energy, $k = 1.4 \times 10^{23}$ J/K is Boltzman's constant, and T is the absolute temperature. The rate of stress relaxation is

$$d\tau/dt = G\, d\varepsilon/dt \tag{5}$$

where G is the shear modulus of the ice. The time required for the stress to relax from τ_1 to τ_2 can be determined by combining these equations, separating variables, and integrating the following:

$$(GC)^{-1}\ \tau^{-3}\, d\tau = dt, \tag{6}$$

which gives

$$t_2 - t_1 = (\tau_1^{-2} - \tau_2^{-2})/2C \tag{7}$$

In freshwater ice with a shear modulus of 4 GPa, this equation yields a relaxation time from 200 to 20 kPa of around 20 hours at -2°C, which is consistent with the experimental results reported by Cox and Johnson. The relaxation time for the same stress change at an average temperature of -20°C is, however, several hundred hours in freshwater ice and several thousand hours in sea ice with a shear modulus of 0.5 MPa. Under these conditions, the stresses induced by differential thermal expansion cannot be neglected.

Differential thermal expansion error in a cylindrical inclusion gauge could be minimized by using a gauge material with the same CTE as ice, however, the only materials with a CTE similar to ice are plastics such as acrylic or Nylon. These materials also have an elastic modulus similar to ice and are thus unsuited for a rigid inclusion gauge.

Flat Panel Gauges

The most extensive work on flat panel gauges was carried out by Exxon Production Research in its work on sea ice pressure panels. It was shown that the stress at the center of a thin flat plate, with a stiffness greater than that of the ice in which it is embedded, is equal to the applied far-field stress component normal to the plate (Chen, 1981). The ratio of ice stress to stress in the center of the sensor panel is provided by

$$\sigma_i/\sigma_{sn} = [1 + (HE_i)/(2DE_S)] / [1+H/2D] \quad (8)$$

where E_i is the elastic modulus of ice, E_S is the sensor modulus normal to the sensor, H is the sensor thickness, and D is its width. If the sensor modulus is greater than or equal to the ice modulus, and if the sensor aspect ratio D/H is 40 or more, this expression approaches unity. A high-aspect-ratio panel sensor can thus be used to provide accurate ice stress measurements in sea ice with varying moduli.

An approximate analytic solution for a thin panel sensor response to a biaxial stress field has been presented by Templeton (1981). The sensor response to transverse loads is minimized when the sensor is as thin as possible. For an aspect ratio of 40 and a sensor that has a transverse stiffness lower than the surrounding ice, the transverse sensitivity should be less than 4% of the normal sensitivity. A transversely stiff sensor may have a relatively large transverse sensitivity.

Templeton also determined the differential thermal expansion sensitivity of a flat panel stress sensor. This sensitivity is minimized when the transverse stiffness of the sensor is less than or equal to that of ice and is independent of the stiffness of the sensor in the sensing direction. The error under these conditions is given by

$$d\sigma_T/dT = k\, E_i(CTE_i - CTE_S) \quad (9)$$

where k is about 0.04. For a steel gauge this amounts to an error of about 1.3 kPa/°C.

The difficulty with this technique is observing the stress in the panel. The strain gauge diaphragms used by Exxon (Chen, 1981) are quite large, and strain gauges are temperature sensitive and subject to drift. Fluid-filled diaphragm (FFD) gauges developed for geotechnical use have also been used to monitor ice stress (Lau and Knoke, 1991). These gauges might be designed to provide a reasonable match to the ice stiffness while limiting transverse sensitivity errors. However, a detailed evaluation of the response of this type of gauge to temperature changes, biaxial stress state, and ice creep has not been carried out.

EMBEDDED OPTICAL FIBER ICE STRESS SENSOR

Optical fiber sensing techniques offer the opportunity to provide high sensitivity, stability, and bandwidth in a very small sensor. At the beginning of this project, a variety of optical techniques were reviewed to arrive at a means of observing stress in the thin panel or rigid cylinder gauge configurations. A report describing this design review is included as an Appendix. The original technique proposed for this work involved the observation of variations in scattered light from an optical fiber mounted close to a moving surface. While this technique is sensitive to dynamic motions, it was found that it is subject to drift when employed for long-term measurements. Other techniques reviewed included interferometry and microbending. None of the existing techniques found in the literature offered the sensitivity and simplicity required for a practical gauge. A new technique based on stress-induced birefringence in optical fibers was therefore developed.

When an optical fiber is subjected to differential stresses the index of refraction in the fiber in the direction of the principal stress is altered. A compressive stress causes the index of refraction to increase slightly. If circularly polarized light is transmitted through the fiber, it becomes elliptically polarized with a phase angle that is linearly related to the applied load. If the light exiting the fiber is analyzed with a polarizing beam splitter, the ratio of the two light intensities can be related to the applied load. This effect has been used to observe bending strains in fibers as a sensing mechanism for a displacement sensor (Imai and Ohtsuka, 1986). The sensing principles for an embedded fiber sensor based on polarized light are described in the following sections.

Stress in an Embedded Optical Fiber

The fiber may be embedded in a panel for the ice stress sensor application as shown in Figure 1. The panel may be cast from a polymer, which minimizes the differential thermal expansion stress and which matches the modulus of the ice. The relationship between principal stresses on a cross section of a circular fiber embedded in a material (σ_{1o} and σ_{2o}) with principal stresses at infinity (σ_1 and σ_2) are given by.

$$\sigma_1 = C_1\sigma_{1o} + C_2\sigma_{2o} \quad \text{and} \quad \sigma_2 = C_2\sigma_{1o} + C_1\sigma_{2o} \tag{10}$$

with

$$C_1 = [k(\chi+2)+\chi_o]/[2k(\chi+1)] \tag{11}$$

$$C_2 = [\chi_o-2-k(\chi-2)]/[2k(\chi+1)] \tag{12}$$

$$k = G_o/G \tag{13}$$

$$\chi = (3-4\nu) \tag{14}$$

where G and G_o are the shear moduli of the panel material and the fiber, and ν is Poisson's ratio. If the minor principal stress is zero and Poisson's ratio equals 0.25 these equations simplify to

$$\sigma_{1O}/\sigma_1 = 3k/(2k+1) \tag{15}$$

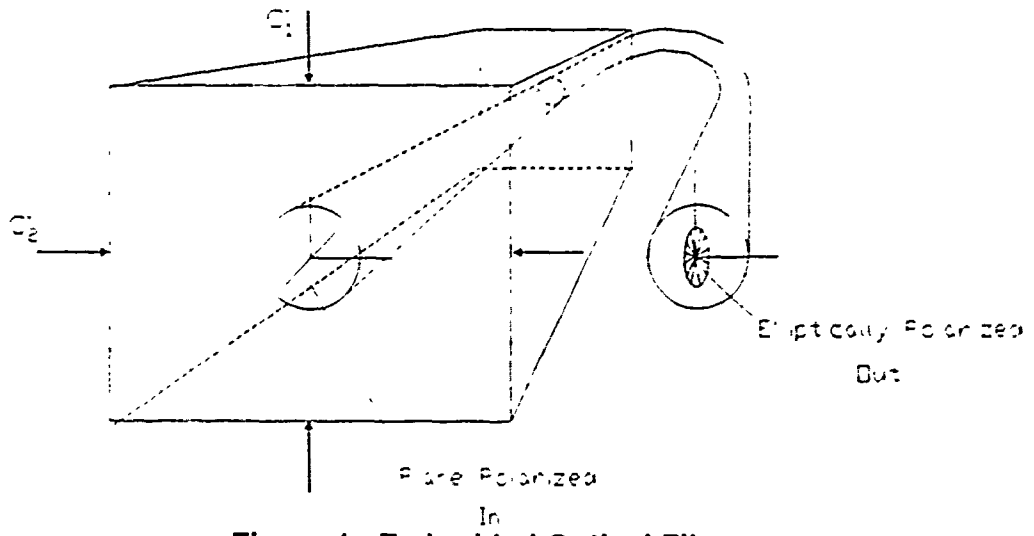

Figure 1. Embedded Optical Fiber

Stress-Induced Birefringence

The differential stress causes a difference in path lengths between the components of the polarized light wave parallel to the applied stress and the perpendicular component. The path difference is related to the length of the fiber, L_f, and the stress-induced birefringence, B:

$$\Delta = L_f B, \tag{16}$$

where

$$B = (\sigma_{1o} - \sigma_{2o})C \tag{17}$$

and C is the stress-optic coefficient of the fiber material ($C_{glass} \cong 3.4 \times 10^{-12}$/Pa; Varnham et al., 1983).

Observation of Birefringence

The stress-induced birefringence may be measured using a technique developed for optical crystallography (Bloss, 1961). An optical schematic of a load sensor based on this technique is shown in Figure 2. Plane polarized light enters the sensor at an angle of τ to the principal stress direction. If the light is analyzed at an angle ϕ to the polarizer, then the intensity is

$$I = \cos^2\phi - \sin^2(\tau-\phi) \cdot \sin 2\tau \cdot \sin^2(\pi\Delta/\lambda) \tag{18}$$

where λ is the light wavelength. In the EOF stress gauge application, the light exiting the detector is split with a polarizing beam splitter into components parallel and perpendicular to the principal polarizer stress and observed with photodetectors. The observed intensity of light parallel to the source polarization is

$$I_1 = I_o \cos^2(\pi\Delta/\lambda) \tag{19}$$

and the intensity of the perpendicular polarization will be

$$I_2 = I_o \sin^2(\pi\Delta/\lambda) \tag{20}$$

The difference and sum of these light intensities gives the sensor signal:

$$(I_1-I_2)/(I_1+I_2) = \cos(2\pi\Delta/\lambda) \tag{21}$$

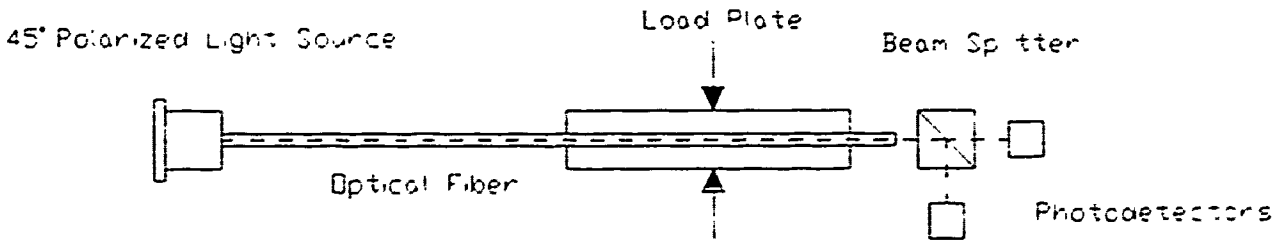

Figure 2. Load Cell Optical Schematic

The amplitude ratio measurement technique provides a signal that is insensitive to variations in light source intensity or other losses in the light transmission system. These variations are the primary cause of long-term drift and temperature sensitivity in amplitude-sensitive optical sensors.

If the source polarization enters the sensor at some other angle or with a different phase retardation, the stress-induced phase retardation will be affected according to Equation (18). Figure 3 gives the theoretical signal value as a function of differential stress in the fiber over a length of 25 mm. The effect of changing the launch polarization angle, τ, is also shown. At a launch angle parallel with one of the principal stress directions, there is no stress-induced retardation. Changing the analyzer angle has the effect of changing the phase of the signal for a launch angle of $\pi/4$. At other launch angles, the analyzer angle affects the sign and amplitude of the observed signal, as shown in Figure 4.

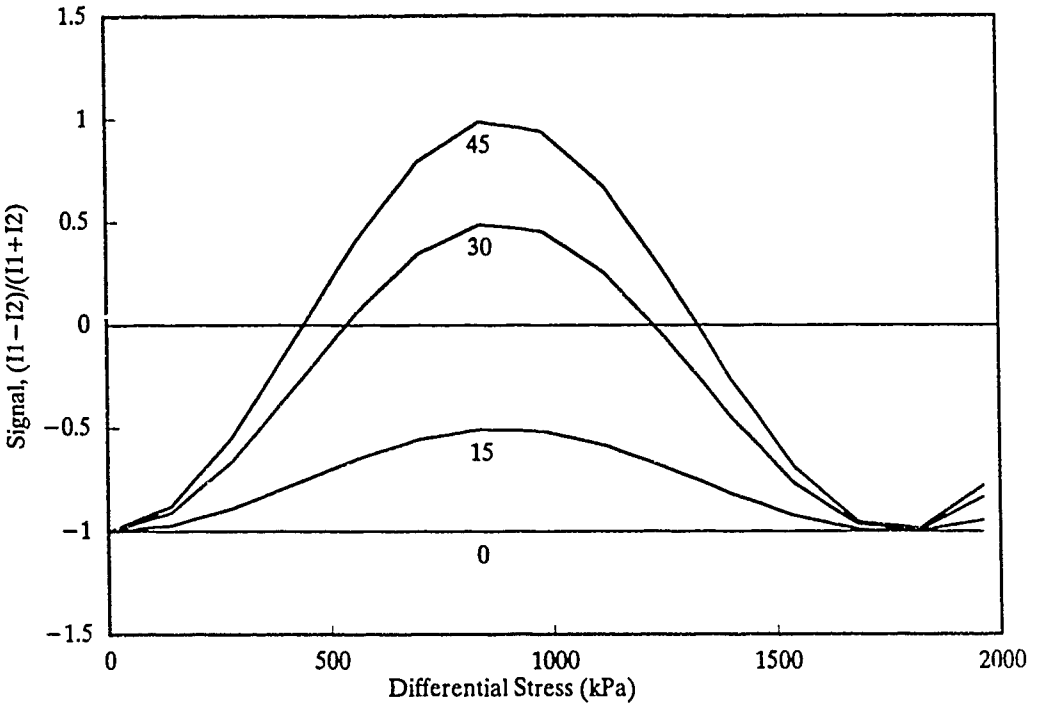

Figure 3. Theoretical Polarimetric Ratio Signal from a 25-mm Embedded Fiber Stress Sensor Showing Effects of Polarizer Launch Angle

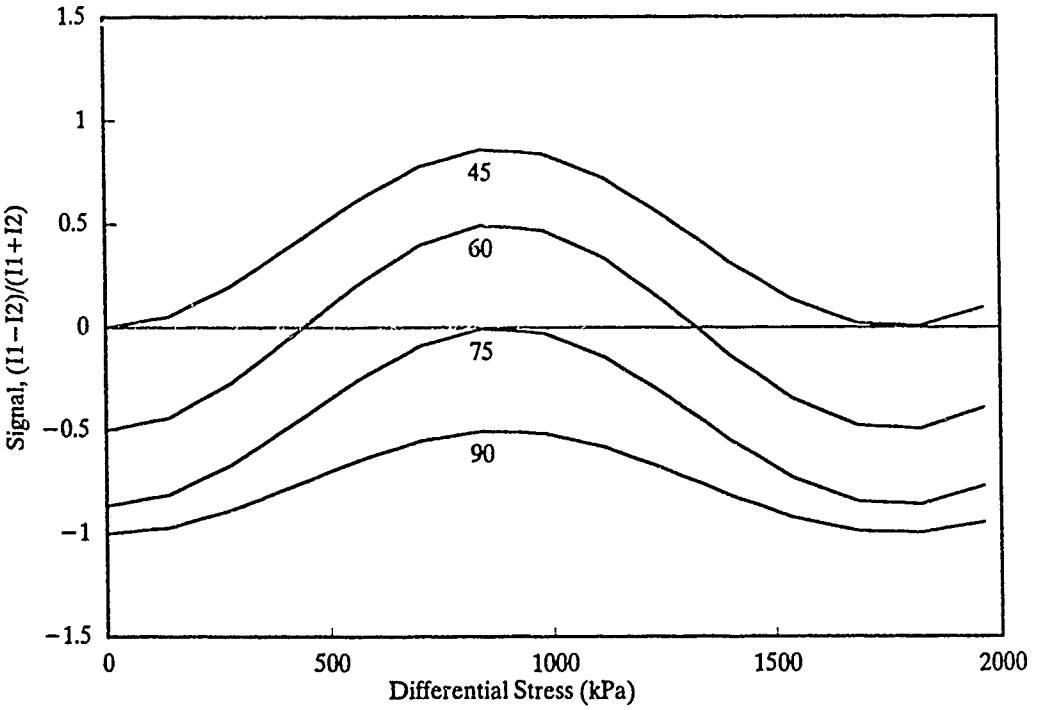

Figure 4. Analyzer Angle Effects on Polarimetric Ratio Amplitude

GAUGE DESIGN AND MATERIAL EVALUATION

A variety of potential gauge panel materials were evaluated in order to obtain an elastic modulus and thermal expansion coefficient that match those of sea ice. Table 1 provides the range of properties of sea ice along with aluminum, steel, and five candidate materials for the stress gauge panel.

Table 1. Stress Sensor Candidate Material Properties

Material	Modulus (GPa)	CTE (10^{-6}/°C)	dCTE (10^{-6}/°C)
Sea Ice Range	0.1 to 7	50	0
Steel	207	17	33
Aluminum	75	24	26
Acrylic	2.8	81	31
High Shock Phenolic	6 to 10	29 to 40	10 to 21
Polyimide	3.3 to 5.3	45 to 50	0 to 5
Cast Polyester	0.7 to 6.3	70 to 101	20 to 51
Bisphenol A Epoxy	3	59	9

Square test panels, 25 mm on a side, were fabricated from Acrylic, polyester, and epoxy. The panels were then placed in an instrumented vise between two 6-mm-thick squares of rubber and loaded up to 1400 kPa in compression. A He-Ne laser was used with a polarizing filter as the source of plane polarized light for the optical setup, shown schematically in Figure 2. The setup varied from the ideal in that both the inlet and outlet fibers were subject to bending. Fiber bending results in birefringence and a consequent retardation (Imai and Ohtsuka, 1986). These changes cause errors in the polarization angle and in the analyzer angle, ϕ.

Welded Acrylic Sensor

The first embedded fiber sensor was fabricated by placing a jacketed fiber between two thin Acrylic plates and welding them together with methylene chloride solvent. The jacket material on the test fibers was also Acrylic, so the result is a fiber embedded in an Acrylic panel. Single-mode, 3-micron core, 125-micron-cladding-diameter, low-birefringence fibers were used for these tests.

Various fiber lengths were achieved by looping the fiber through the sensor. This results in bending stresses in the sensor itself. In these tests the outlet fiber was twisted until the two polarization intensities were approximately equal at zero load.

Figure 5 shows the results of three load tests of the welded Acrylic sensor. The sensitivity of the sensor increases with fiber length as expected, but the relationship is nonlinear, particularly at higher loads. This is thought to be a consequence of phase angle changes induced by fiber binding. The output signal was also found to be subject to severe creep, the signal at a constant load was found to drift back to zero

after a few hours. Acrylic is known to be subject to creep at low loads, and this behavior may be exacerbated by the solvent used for welding. Attempts to bake the sensors to drive off the solvent did not appear to reduce the creep drift problem.

Cast Polyester and Epoxy Sensors

Polyester and epoxy were chosen for further experimentation because of the ease with which they can be cast. These materials are also known to have much lower creep rates at low loads than Acrylic. A 25-mm-square by 3-mm-thick casting mold was prepared for these tests from a urethane tooling compound. Optical fibers were prepared by stripping the Acrylic buffer jacket from the fiber over a 25-mm-long section. The bare fiber was held in place in the mold and the casting compound poured around it.

Both single- and multiple-mode fibers were cast into a clear polyester casting compound and a Bisphenol A rigid casting epoxy. The epoxy panel with two embedded fibers is shown in Figure 6.

The single-mode polyester sensor response is shown in Figure 7. The two curves show the retardation phase shift caused by twisting the outlet fiber. A phase retardation of π is generated by an induced stress of about 1 MPa. The multimode fiber response is shown in Figure 8. The multimode curves show a greater effect of fiber twist and bending on the amplitude of the response.

The cast epoxy sensor response is very similar to that of the polyester sensor, which is not surprising since the elastic modulus of these materials is similar. Figure 9 shows the single-mode fiber response, and Figure 10 shows the multimode response. The large hysteresis in Figure 10 shows the sensitivity of multimode fibers to small environmental changes.

Both single-mode sensors were also tested for creep response at an applied stress of 700 kPa for one hour. Under these conditions, the polyester sensor was observed to drift downwards by a phase angle of 0.31 rad while the epoxy sensor drift was only 0.11 rad. Total creep of the epoxy sensor after 3 hours was 0.15 rad, which is less than 4.5% of the full range (π rad).

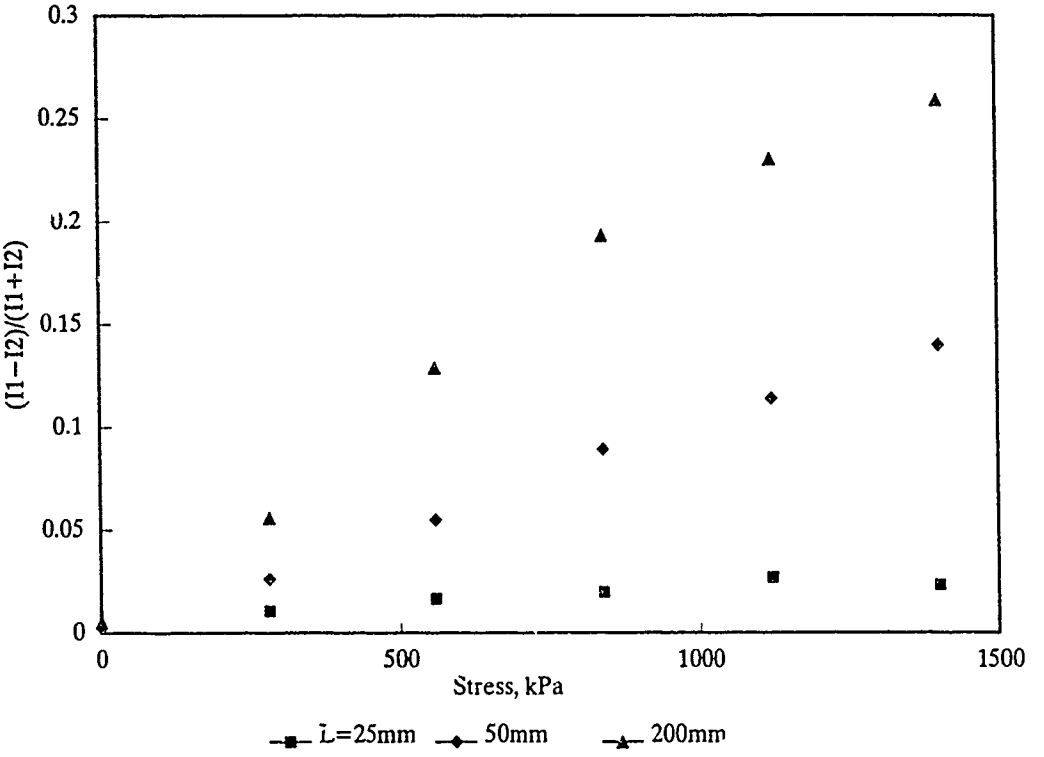

Figure 5. Welded Acrylic Sensor Response Showing Effect of Fiber Length

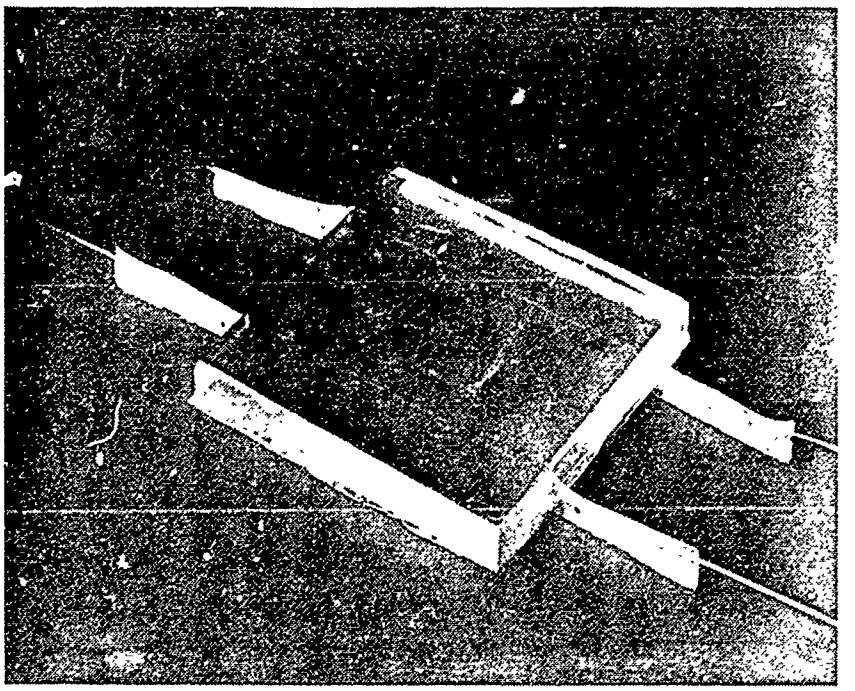

Figure 6. Cast Epoxy Test Sensor; Embedded Single- and Multimode Optical Fibers

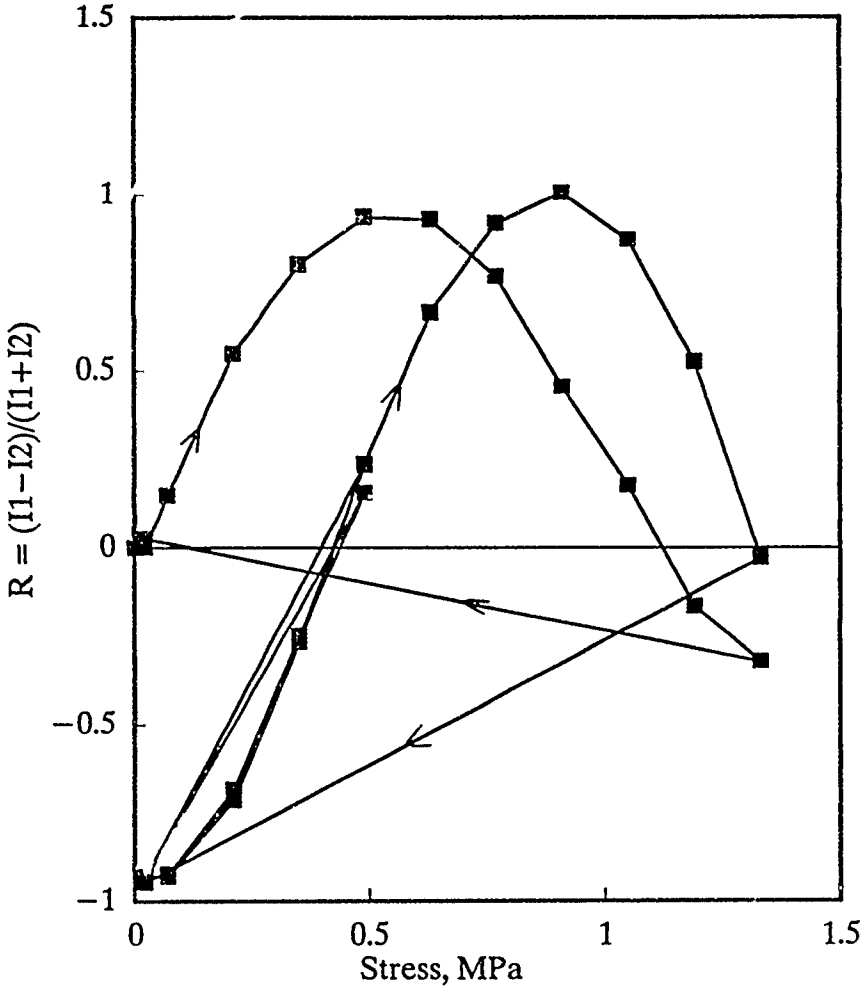

Figure 7. Cast Polyester Sensor; 28-mm Single-Mode Fiber Response

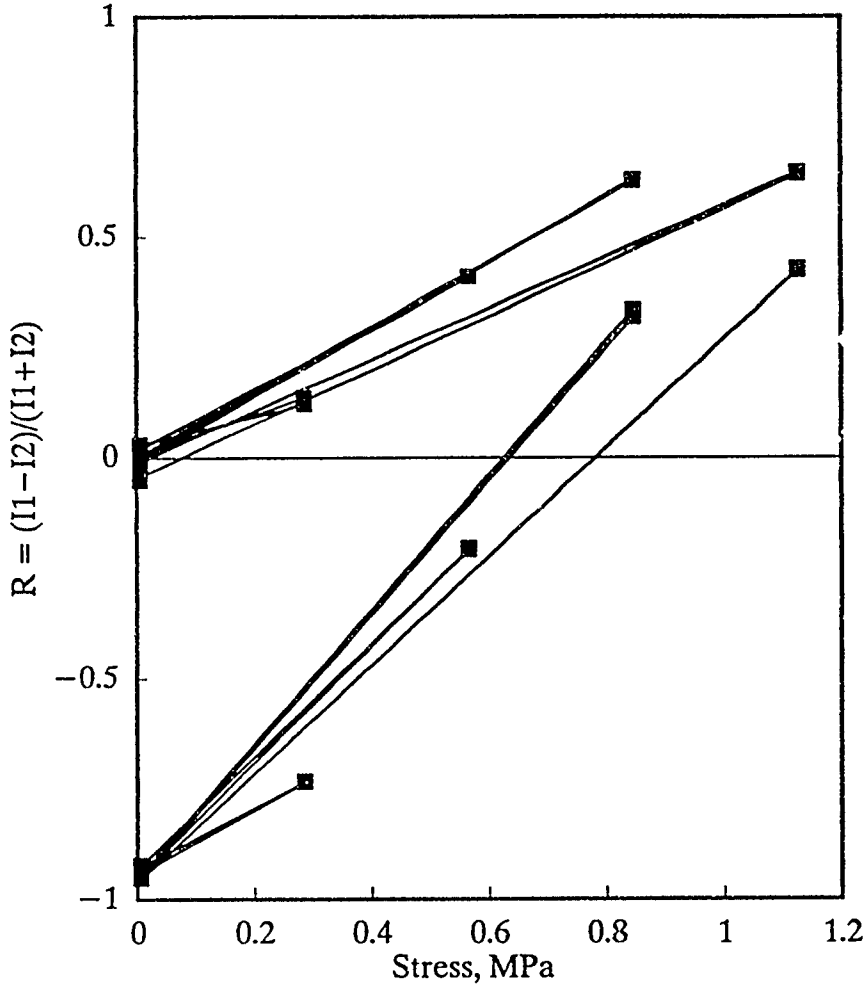

Figure 8. Cast Polyester Sensor; 28-mm Multimode Fiber Response

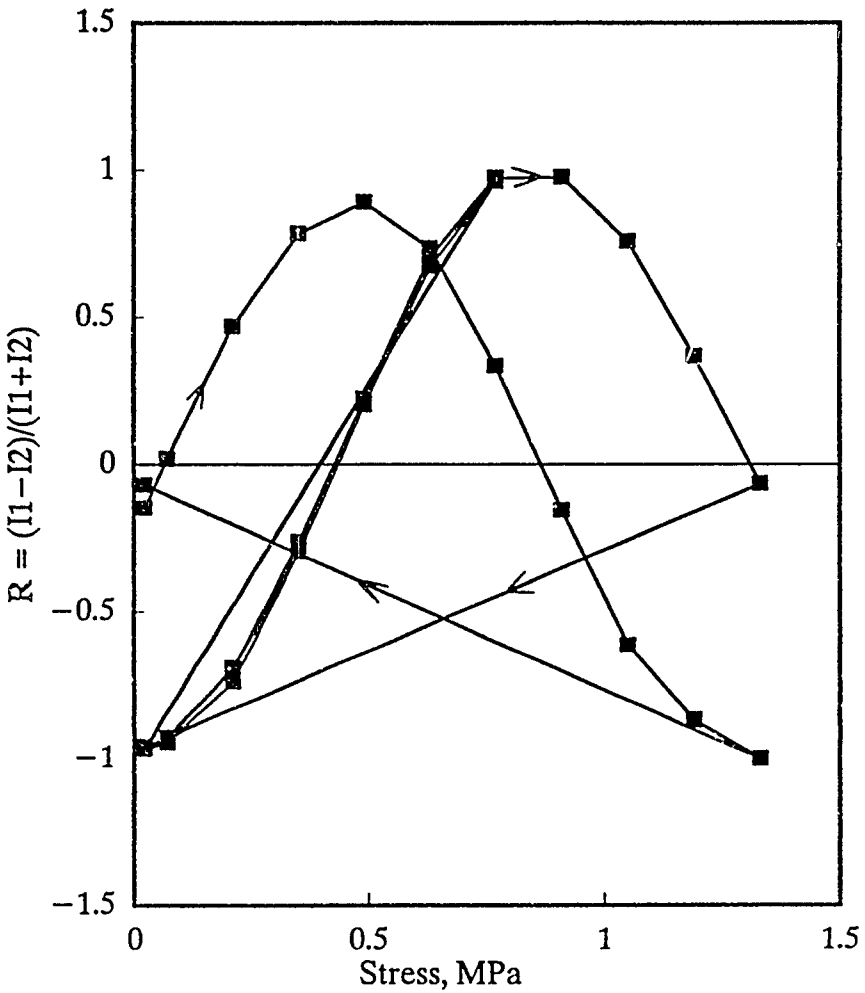

Figure 9. Cast Epoxy Sensor;
28-mm Single-Mode Fiber Response

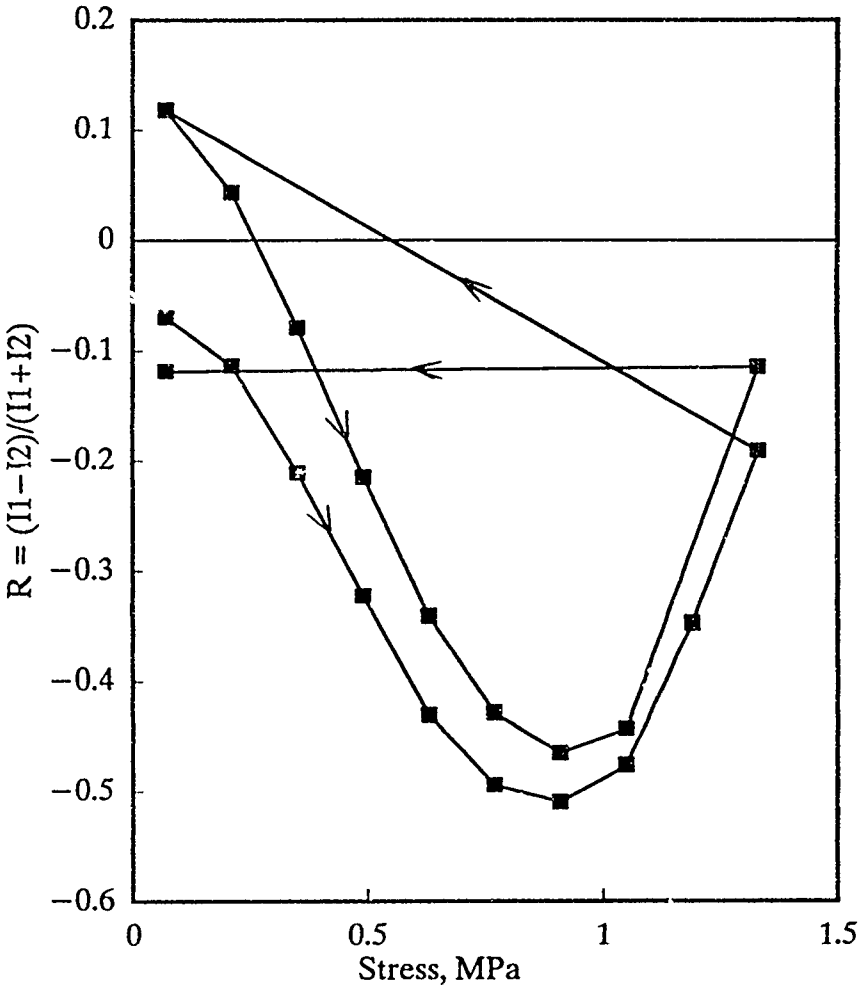

Figure 10. Cast Epoxy Sensor;
28-mm Multimode Fiber Response

ICE STRESS OBSERVATIONS

The initial testing with 25-mm panels in a vise showed that the embedded optical fiber could be used to measure stress over the range of up to 500 kPa found in sea ice. Further work then focused on designing and fabricating an embedded panel gauge suitable for deployment in ice. A gauge was fabricated, embedded in ice, and tested in a load frame using the same benchtop optical configuration used previously. Ice stress tests were carried out to evaluate sensitivity, accuracy, and ice creep effects. Further tests on this sensor were carried out to evaluate long-term drift and thermal response.

Ice Stress Gauge Fabrication

Epoxy was chosen as the material for further testing because of its lower creep. Multimode fibers are less expensive and may be coupled to inexpensive light sources, however, the larger core diameter means that some modes are easily outcoupled from the fiber due to bending. Mode outcoupling is also sensitive to polarization angle. Single-mode fibers are less sensitive to bending-induced outcoupling and were selected for further testing because of the greater repeatability of test results as compared to multimode fibers.

An 80-mm-square mold was prepared for casting 2-mm-thick panels of epoxy. A 25-mm section of single-mode fiber was stripped of its jacket with solvent and placed in the mold. The remaining fiber was placed inside a 1-mm Teflon tube, which acts to isolate the lead fibers from applied stress. Epoxy was cast into the mold resulting in the sensor panel shown in Figure 11. A square of polyester fabric was then glued to both surfaces of the panel to provide mechanical bonding with the ice. The optical fiber leads were further protected inside a 25-mm Acrylic tube..

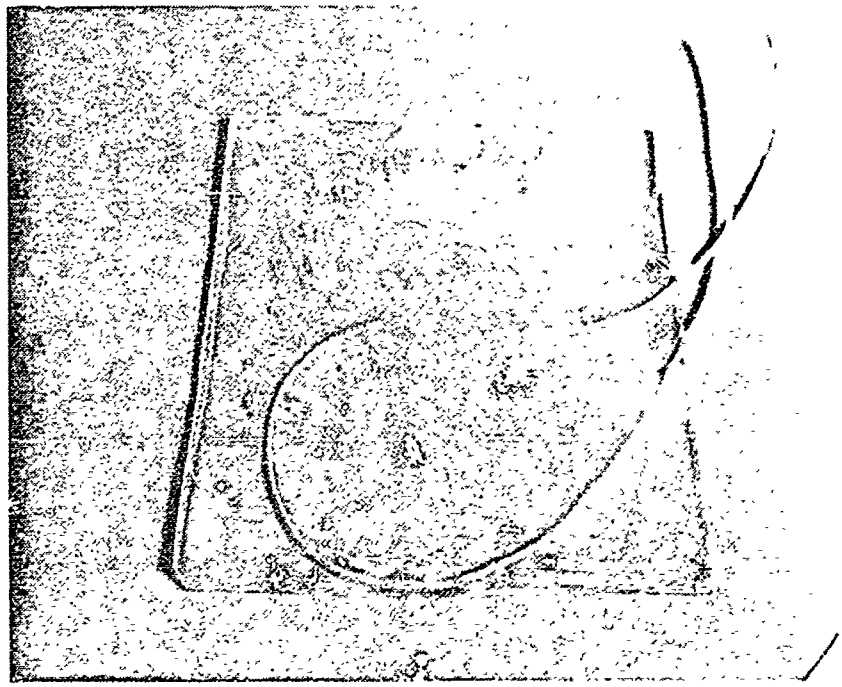

Figure 11. Cast Epoxy Stress Gauge; 25-mm Sensitive Section of Bare Optical Fiber in the Center

Load Frame and Test Configuration

The sensor was embedded in a 300-mm-square, 150-mm-thick block of ice formed by freezing crushed ice and water. The ice block was frozen in place in a uniaxial load frame located in a top loading freezer, as shown in Figure 12. The freezer was equipped with a fan to maintain a uniform temperature of about -20°C. Load was applied manually with a hydraulic jack and monitored with a pressure gauge. Errors in controlling the pressure limit the accuracy of the applied values presented here to ±20 kPa.

The fibers were led up out of the freezer to a He-Ne laser light source and to a split prism polarization analyzer, shown in Figure 13. This sensor configuration is designed so that the sensitive fiber is oriented horizontally in the ice test block. Since the vertical stress is zero in this orientation, only the stress normal to the panel should contribute to fiber birefringence.

The inlet polarization was vertical in all of the tests, and the laser was oriented at 45° to the plane of the sensor. The optical system was aligned by observing the outlet polarization at zero load. The bending of the optical fiber path results in a phase shift before the light enters the sensitive section of the gauge and after it exits this section. These effects may be compensated for, to some extent, by bending the fiber as it exits the laser until the vertical polarization of the light is maximized at the analyzer. This was always possible in practice with the single-mode fiber sensors. The outlet fiber may then be twisted to arrive at any desired zero load phase angle.

Normal Load Sensitivity and Support Tube Effects

The first set of load tests was carried out with the sensor oriented normal to the uniaxial load. The phase retardation angle at zero load was set to be about -0.8 rad by twisting the outlet fiber. Loads were applied manually and held for 30 seconds for each point.

An initial series of tests was carried out with the sensor loaded in both tension and compression. Figure 14 shows the tensile and compressive load curves over a low load range. Notice that the sensitivity in this case is approximately equal to the vise loading tests. 3.0 rad/MPa. At higher loads, as shown in Figure 15, the sensitivity is the same but some hysteresis is apparent in the sensor response curves.

The sensor was then removed from the ice to change the support tube configuration from a 25-mm Acrylic tube to a 9-mm Teflon tube. It was thought that the larger-diameter support tube might be creeping or otherwise contributing to the observed hysteresis. An improved data acquisition system with lower noise was also used in subsequent tests.

Figure 16 shows the response to compressive loading to 500 kPa followed by unloading. The response is linear during both loading and unloading but shows significant hysteresis. A similar curve, limited to 85 kPa, is shown in Figure 17. The normal sensitivity of the sensor is 2 rad/MPa, 30% lower than that observed with the larger support tube. As discussed previously, variations in sensitivity are a function of the inlet polarization angle, which may in turn be changed by inlet fiber bending. An increase in inlet fiber bending severity in the smaller support tube is likely responsible for the observed decrease in sensitivity.

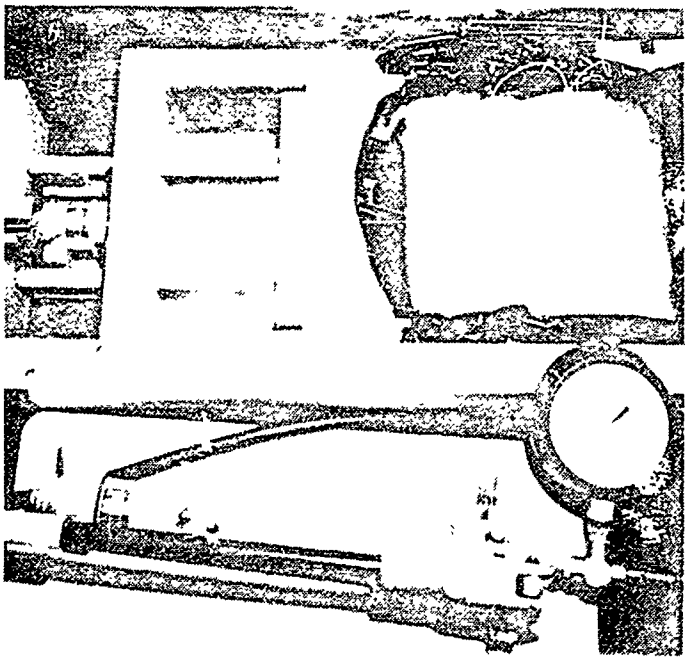

Figure 12. Load Frame Showing Hydraulic Load Ram in Tensile Load Position, Ice Block with Emerging Optical Fiber Leads, and Thermocouple Leads

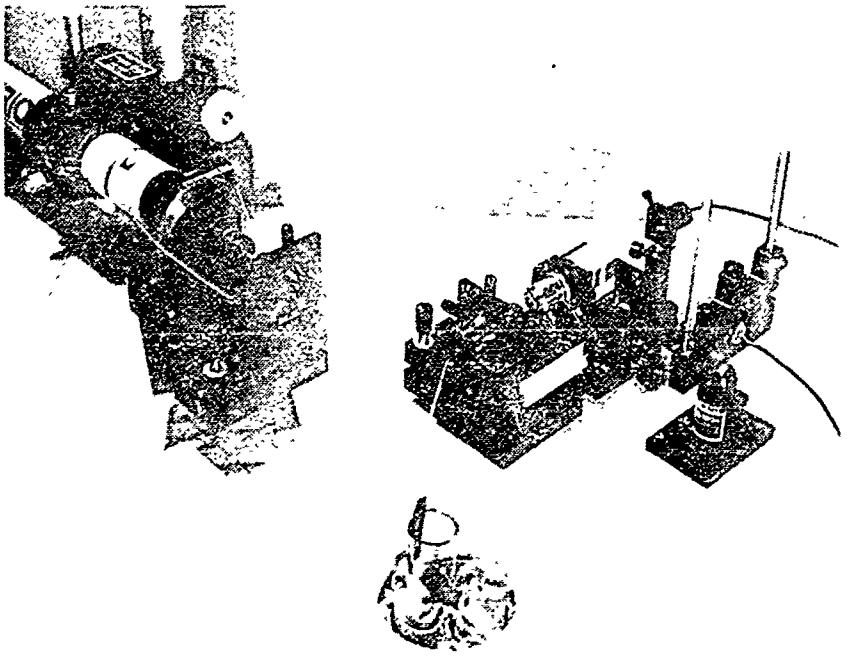

Figure 13. Freezer Top Optical Setup Showing He-Ne Laser, Polarizer, Fiber Couplers, Inlet and Outlet Fibers, Polarization Preserving Beam Splitter, and Matched Photodetectors

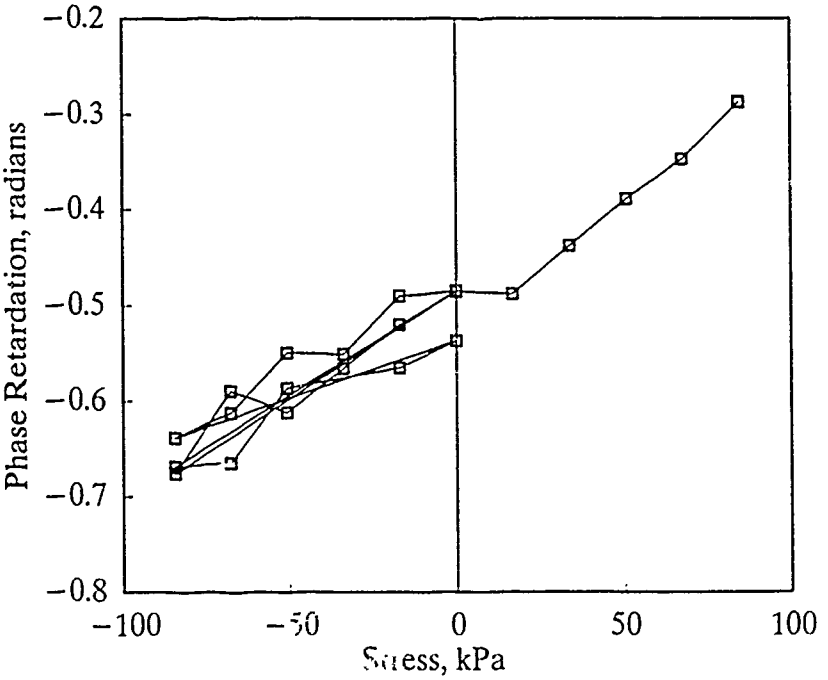

Figure 14. Sensor Response to Tensile (-) and Compressive (+) Loading and Unloading; 25-mm Acrylic Support Tube

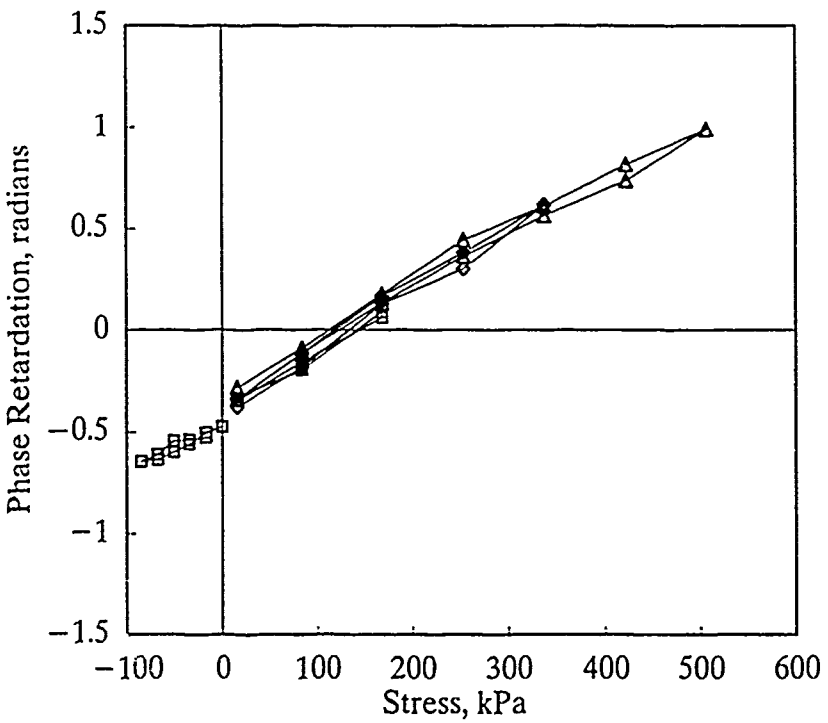

Figure 15. Sensor Response to Low-Level Tensile (-) and Compressive (+) Loading; 25-mm Acrylic Support Tube

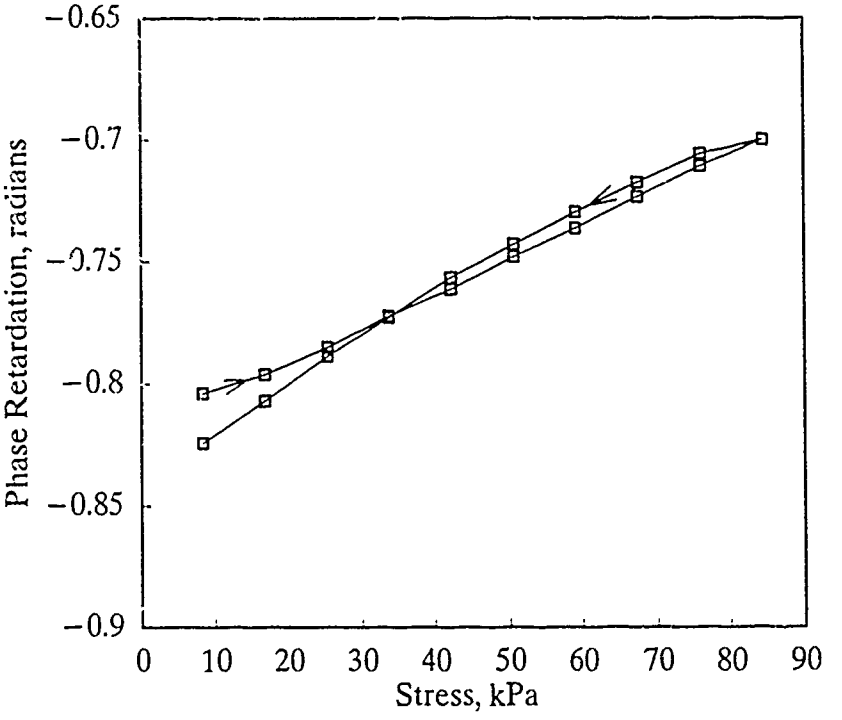

Figure 16. Sensor Response to Full-Scale Compressive Load; 9-mm Teflon Support Tube

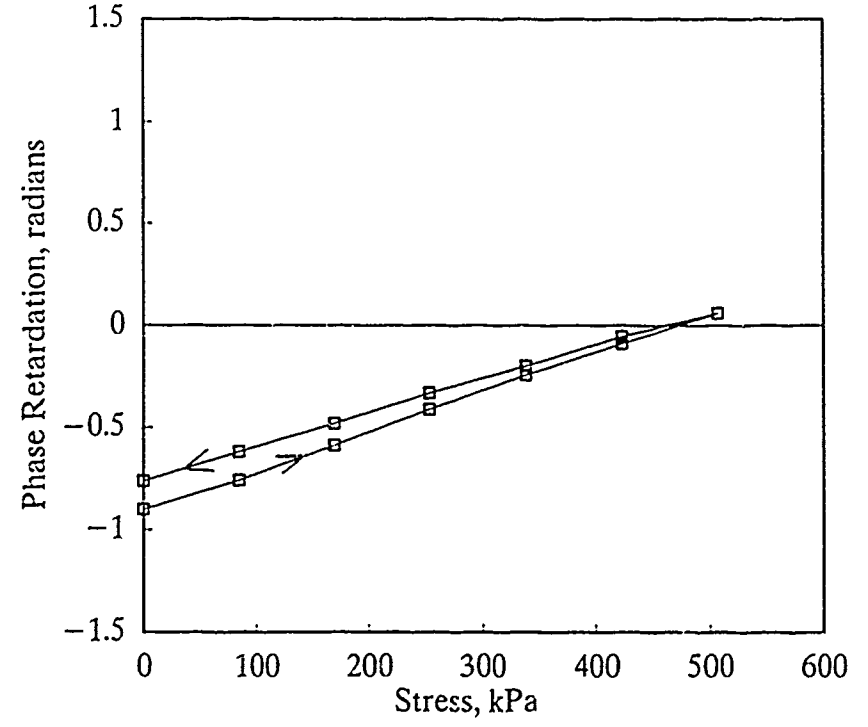

Figure 17. Sensor Response to Low Level Compressive Loading; 9-mm Teflon Support Tube

Transverse Load Sensitivity

The sensor was next embedded in the ice parallel to the uniaxial stress direction. Since it is possible to reduce sensor sensitivity by changing the inlet polarization, a variety of initial polarization conditions was used to test for transverse sensor sensitivity. The results of several load tests with various inlet and outlet twists to vary the initial phase angles are shown in Figure 18. The maximum transverse sensitivity observed was -0.2 rad/MPa, which amounts to 10% of the normal sensitivity for this sensor configuration.

Creep

The effects of sensor creep during these tests was masked by ice creep effects.. Figure 19 shows an extreme example of this hysteresis at high loads. Note that the unloading signal is higher than the loading curve. This result is opposite to the effect of sensor material creep, which causes the signal to decay with time towards the zero load level. The observed hysteresis is apparently due to ice creep. As the ice creeps around the sensor, it causes a tensile load in the vertical transverse direction. This results in an increased differential stress and a continual upwards creep in the signal.

Drift, Precision, and Resolution

The signal variation, due to sensor drift during two drift experiments, is shown in Figure 20. Sensor drift was first observed at zero load by leaving the sensor in place for 60 hours. The standard deviation of the output signal over this period was 0.016 rad or about 9 kPa. The signal variation is apparently correlated to daily variations in room temperature. These changes may cause sufficient changes in the fiber bending, enough to cause the observed long-term drift signal.

A second drift experiment was carried out at a constant load of 170 kPa. This experiment was carried out after reloading the sensor into a cavity melted out of the center of the ice block. Initial stresses in the sensor were quite high because of the expansion of the freezing ice in the cavity surrounding the sensor within the ice block. The drift data show the initial variation in the signal as the ice creeps. After 250 hours, the signal has a variation of .16 rad, corresponding to 90 kPa. The source of this drift error may be continued relaxation of thermal stress, long-term mechanical creep at the optical couplers, or some creep mechanism in the sensor itself.

The precision and resolution of the sensor signal was obtained by taking a series of data at intervals of 10 seconds. This procedure resulted in a standard deviation in signal of 0.0008 rad, corresponding to a resolution of 0.4 kPa. This resolution is limited by the noise level in the photodetector and amplifier circuitry as well as the vibrations of the optical equipment and fibers.

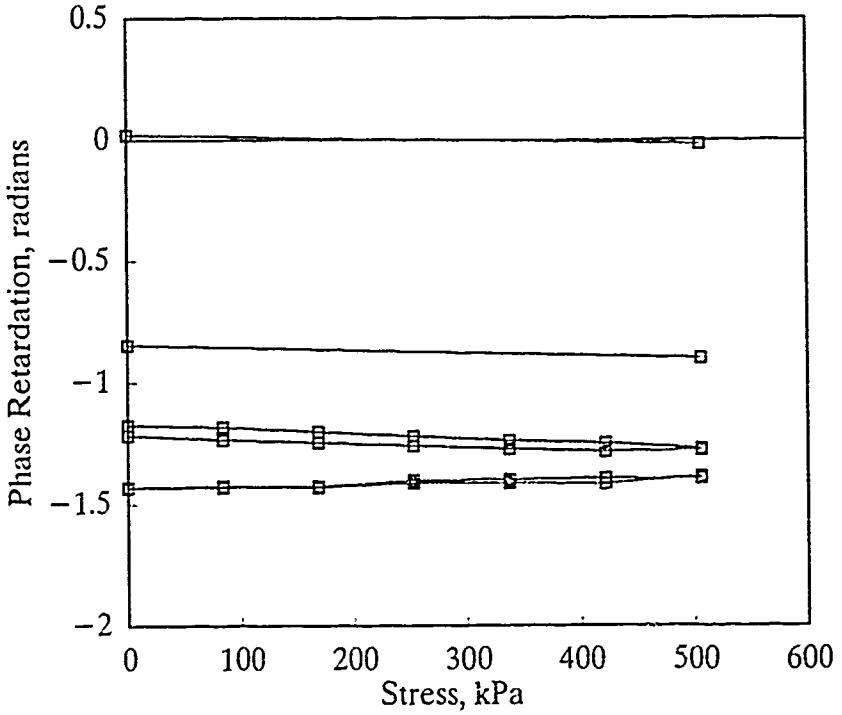

Figure 18. Transverse Load Response Showing Effects of Various Inlet and Outlet Fiber Bending Conditions

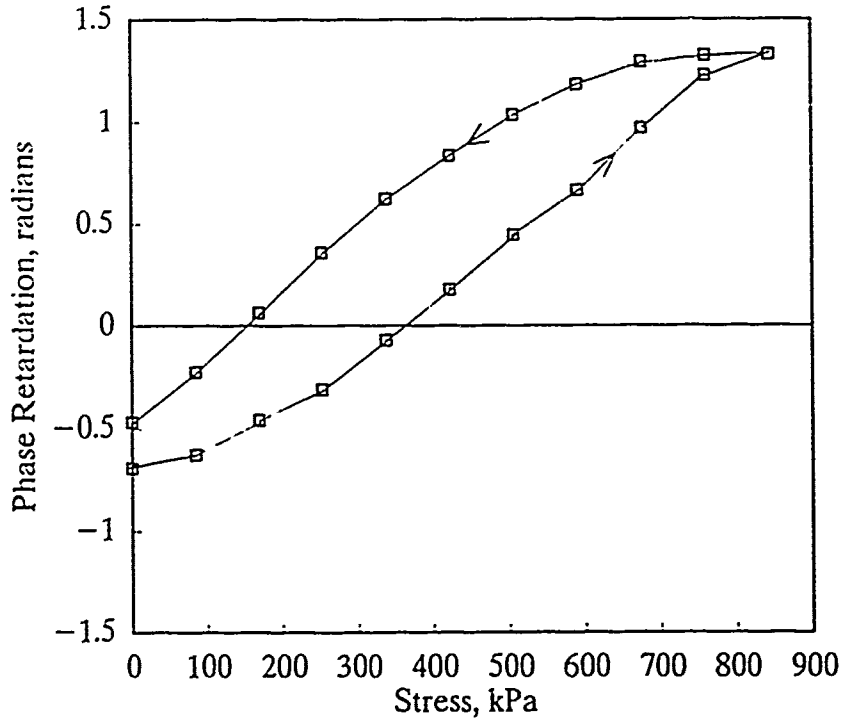

Figure 19. Sensor Response Hysteresis Due to Ice Creep

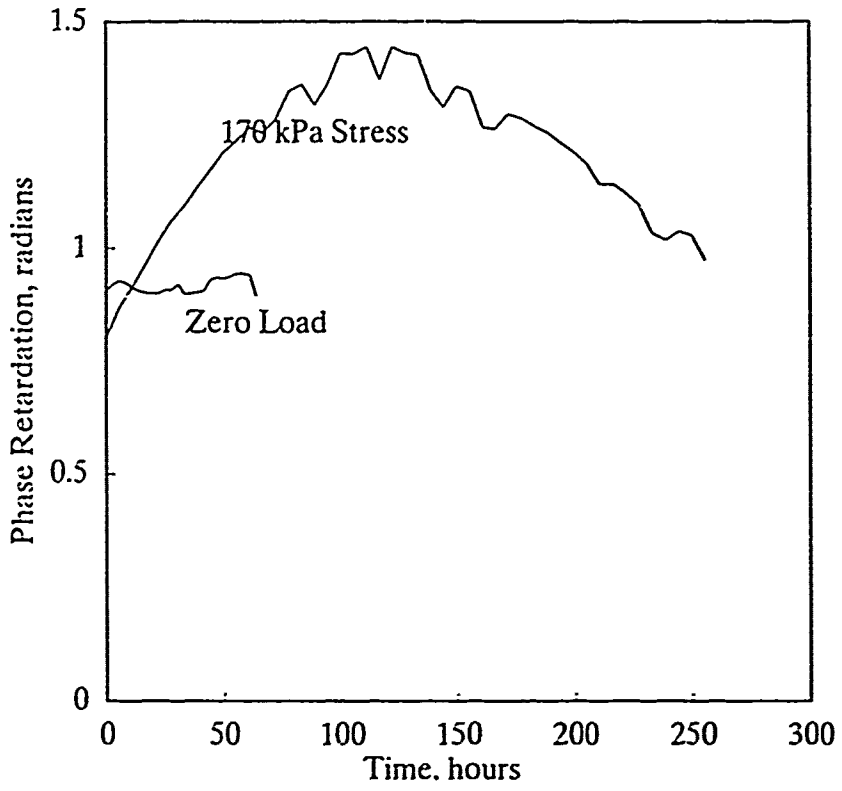

Figure 20. Sensor Drift at Zero Stress and at 170-kPa Constant Stress

Thermal Response

The thermal response of the gauge was evaluated by changing the temperature of a water bath from 3.5°C to 46°C. The mean response observed with this procedure over four trials was -0.0059±0.0006 rad/°C. This corresponds to a thermal error of -3 kPa/°C.

GAUGE DESIGN FOR FIELD DEPLOYMENT

The benchtop demonstration of the EOF gauge concept relied upon an external, visible laser light source with macroscopic fiber couplers, a beam splitter, and detectors. This optical setup is sensitive to vibrations, air currents, room temperature, and other environmental conditions because of the length of fiber required. A gauge suitable for field deployment would use integrated optics with a small fixed fiber length to minimize drift and precision errors associated with long exposed fiber lengths and temperature variations between the optics and sensing region.

Integrated EOF Gauge

A preliminary design for an integrated EOF gauge panel suitable for field deployment is shown in Figure 21. Polarized light for the sensor will be provided by a pulsed diode laser. Infrared lasers with pre-coupled single-mode optical fibers are available commercially for use in communications equipment. The source laser may be oriented directly in line with the sensitive region of the stress panel. This means that the polarization of light entering the sensitive region may be fixed at 45°, thereby fixing the response of all gauges. The fiber will be bent through a 180° semicircle to return to the analyzer, providing a fixed-phase shift to the response, which should also be the same for each sensor.

The analyzer optics will be miniaturized and placed on a small board. An amplifier circuit on the same board would provide a stable output signal based on the difference/sum ratio of the two detector signals.

Estimated material and fabrication bids for a single panel, in quantities of 10 or more, have been obtained from vendors and are shown in Table 2.

Table 2. Estimated Material and Fabrication Costs for an Integrated EOF Gauge Panel in Quantities of Less Than 100

Component	Cost	Vendor
Pigtailed IR Diode Laser with 5/125 Single-Mode Fiber	$315	SeaStar Optics
Analyzer Optronics Board	$300	United Detector Technologies
Epoxy Panel Casting	$70	United Detector Technologies
Total	$685	

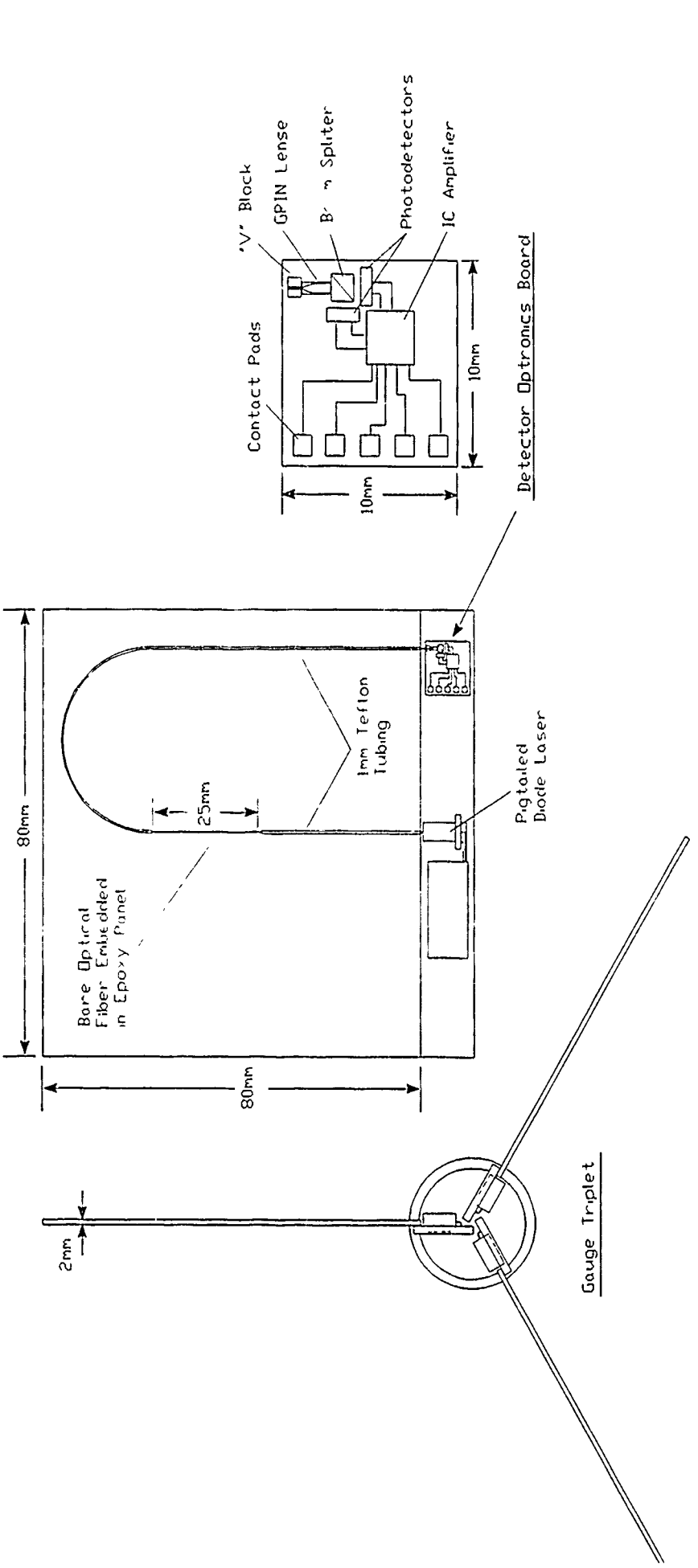

Figure 21. Integrated EOF Stress Gauge Panel

Biaxial Stress Measurements

The flat panel measurement technique yields a single measurement of stress normal to the plane of the gauge. Three gauges oriented at different angles are required to determine the two principal horizontal stresses and their orientation. The flat panel gauges perturb the stress field only near the edges of the gauge. The deployment must therefore balance the desire to obtain a stress measurement at the same point with the need to space the gauges so that they do not interfere with each other. The region of interference is minimized when the gauge stiffness matches the ice stiffness. Chen (1981) has calculated the stress field perturbations around the edges of a thin panel gauge. A gauge with a stiffness within a factor of 10 of the surrounding ice will disturb the stress field at a radius from the edge of the gauge limited to about 20% of the gauge width. This implies that the gauges may be located close together.

A plan for a gauge triplet deployment is illustrated in Figure 22. Mounting from a central support post will allow rapid deployment of a vertical array of gauge triplets with identical gauge orientations, thus simplifying deployment and data reduction. The support post will also perturb the stress field at a radius proportional to its diameter and the stiffness mismatch. The final design of this mounting will require a numerical analysis of the stress field perturbation to ensure that the sensitive region of the gauge is far enough from the gauge support.

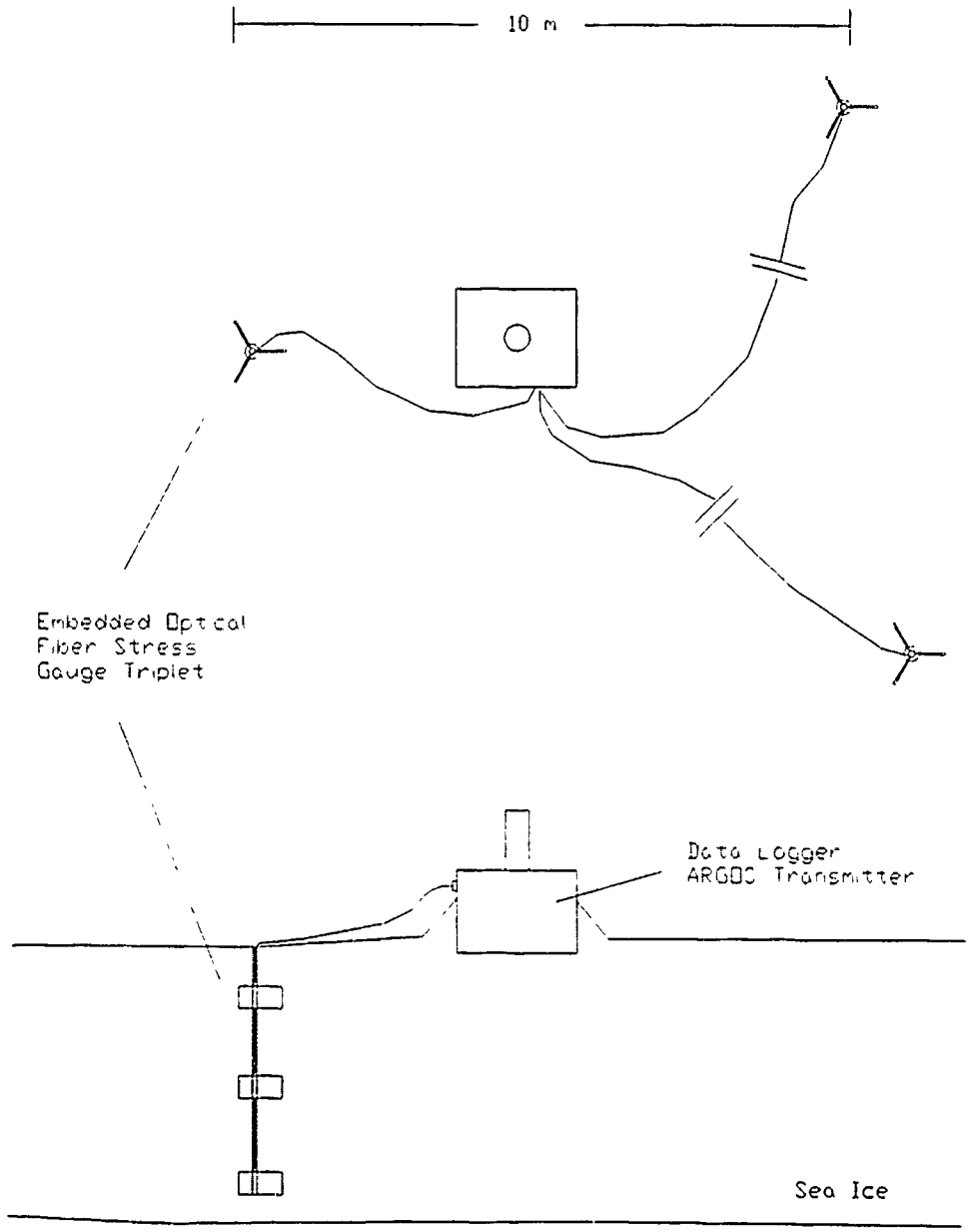

Figure 22. EOF Gauge Triplet Deployment Scheme

SUMMARY AND CONCLUSIONS

A summary of the embedded optical fiber gauge performance characteristics is provided in Table 3. The performance of the gauge developed for the feasibility demonstration may be compared to the specifications provided in Table 4 for two gauges that have been in recent use for the observation of floe-scale and geophysical-scale stresses in sea ice. The benchtop demonstration gauge has demonstrated a resolution and range comparable to that of the FFD. The transverse sensitivity is low, and the gauge drift at zero load over long periods has been demonstrated to be comparable to, or lower than, existing gauges. Gauge hysteresis due to ice creep was observed, however, this effect can be minimized by increasing the transverse gauge stiffness. The long-term drift observed is due to the type of load applied or the macroscopic optical system or is intrinsic to the sensor itself.

Existing gauges use vibrating wire technology to provide a stable low-drift signal with relative noise immunity suitable for long cable runs. The excitation signal for the vibrating wire is a swept frequency pulse that lasts for about 1 second. The EOF gauge excitation is a pulse of laser light that may have a duration of less than 1 millisecond. The power draw of the EOF gauge is thus much smaller than for existing gauges, which is an important requirement for long-term unmanned measurements at multiple locations. The EOF gauge is also capable of providing data at acoustic frequencies, which may be useful for the observation of floe interactions. The EOF gauge is relatively small and could be deployed at multiple levels in a single borehole.

Finally, the estimated cost of a prototype integrated EOF gauge is comparable to that of existing gauge technology. The user cost for production gauges in larger quantities should be similar. The sensing mechanism may have broader applications, such as sensing broadband acoustic signals or other types of dynamic loading. These sensors would rely upon the same laser source and analyzer optronics. If a very large number of laser diodes and analyzer boards are produced, the individual cost can be quite low.

Table 3. Characteristics of Existing Rigid Cylindrical Inclusion (RCI) and Fluid-Filled Diaphragm (FFD) Stress Gauges

Gauge Type	Rigid Cylindrical Inclusion	Fluid-Filled Diaphragm
Transducer mechanism	Vibrating Wire	Vibrating Wire
Range	-1 to 200 MPa	-100 to 500 kPa
Resolution	20 kPa	0.35 kPa
Transverse sensitivity	Biaxial	not available
Thermal sensitivity	5 kPa/°C	not available
Differential CTE error	25 kPa/°C	9 kPa/°C
Maximum drift	4 kPa/day	1 Pa/day
Accuracy	±15%	not available
Frequency range	DC to Hz	DC to Hz
Inclusion factor	Independent of ice modulus	Independent of ice modulus
Diameter	57 mm	200-mm disks
Deployment	100-mm borehole	Sawcut in a pit
Cost	$1100 for three channels	$2250 for three channels
Power	70 mW for 1-second sweep	70 mW for 1-second sweep
Source	Cox and Johnson (1983)	IRAD/Geokon literature

Table 4. Prototype EOF Stress Gauge Characteristics

Transducer mechanism	Stress-induced birefringence in single-mode optical fiber
Range	-100 kPa tension to 500 kPa compression
Resolution	0.42 kPa (0.0016 rad)
Transverse sensitivity	0.00019 rad/kPa (5.0% of normal sensitivity)
Thermal sensitivity	-3.0 kPa/°C
Differential CTE error	2.5 kPa/°C (maximum theoretical error)
Drift	4.0 kPa/day over 60 hours at zero load, T = ±1.5°C
Accuracy	±10%
Frequency range	DC to MHz
Inclusion factor	Independent of ice modulus
Size	80-mm square panel
Deployment	200-mm borehole
Cost	$2055 for three channels
Power	100 mW for 1-millisecond pulse

REFERENCES

Bloss, F.D. (1961) *An Introduction to the Methods of Optical Crystallography*, Holt, Reinhart, and Wilson, New York.

Chen, A.C.T. (1981) "Transverse Pressure Effects On an Embedded Ice Pressure Sensor," POAC 81, *Proceedings of the Sixth Int. Conf. on Port and Ocean Engineering under Arctic Conditions*, pp. 375-384.

Cox, G.F.N., and J.B. Johnson (1983) "Stress Measurements In Ice," CRREL Report 82-23, U.S. Army Cold Regions Research and Engineering Laboratory, Hanover, New Hampshire.

Hobbs, P.V. (1974) *Ice Physics*, Clarendon Press, Oxford.

Imai, Y., and Ohtsuka, Y. (1986) "Compensated Sensing Based on Retardation Characteristics In a Bent Birefringent Fiber," *J. Appl. Optics*, Vol. 25, No. 23, pp. 4444-4447.

Lau, P.A., and G.S. Knoke (1991) Arctic Ice Stress Measurements, presented at Oceans 91, Honolulu, IEEE, Piscataway, New Jersey.

Templeton, J.S. (1981) "Analysis for an Embedded Ice Pressure Sensor," *J. Energy Resources Tech.*, Vol. 103, pp. 87-95.

Varnham, M.P., D.P. Payne, A.J. Barlow, and K.D. Birch (1983) "Analytic Solution for the Birefringence Produced by Thermal Stress in Polarization-Maintaining Optical Fibers," *J. Lightwave Tech.*, Vol. LT-1, No. 2, pp. 332-339.

APPENDIX

REVIEW OF FIBER-OPTIC STRESS SENSOR

INTRODUCTION

Fiber-optic (F/O) sensors are dielectric waveguide devices and are immune to electromagnetic interference. In their simplest form they comprise a light source, one or more optical fibers, an optical modulation mechanism, a photodetector, and signal processing hardware. The source may be a filament bulb or other blackbody radiator, a light emitting diode (LED), a laser diode, or a nonconventional source such as chemically produced light. The fibers may be step index multimode, step index single-mode, gradient index single-mode or polarization preserving (PP) types. The modulation mechanisms are numerous, and the methods appropriate for measuring ice stress will be discussed below. The photodetector is usually a silicon photodiode, a photomultiplier tube, or avalanche photodiode.

SENSOR REQUIREMENTS

Sensed Quantity

The transduction mechanism for stress is a small displacement. It is anticipated that the outer wall of a pair of coaxial steel cylinders will experience a small displacement due to a ±2 MPa (280 psi) stress applied over a length of the cylinder. The goal for minimum detectable stress is 10 kPa (1.4 psi). Thus the sensor and its support electronics must be capable of at least a 400.1 dynamic range, or expressed in instrument units as 52 db. As currently envisioned, the minimum detectable stress would cause a 0.025-micron movement of the outer cylinder wall. This movement can be made an order of magnitude larger with a smaller wall thickness.

Accuracy

It is expected the measured stress will be accurate to 1% over the temperature range of -10°C to 10°C.

Environmental

The ice stress sensor will be deployed in a quiet, but cold environment. If the selected sensing method is DC, then fiber motions during the measurement process will corrupt the obtained signal. Placement and type of fibers will minimize this error.

SENSING METHODS

Extrinsic and Intrinsic

There are two methods used in the design of F/O sensors for extracting a signal from the environment. The case where the fiber itself serves as the transducer is called an intrinsic sensor. When the light is modulated by some means external to the fiber, the sensor is of an extrinsic type.

Amplitude

An amplitude F/O sensor usually employs multimode fibers, is cheap, and usually is moderately accurate for DC and AC type measurements. A common technique used in amplitude sensing involves the transmission of light across a gap from one fiber to another. This could also be accomplished by reflection off a mirrored surface from two fibers parallel to each other on the same side of the mirror. In this embodiment, one fiber directs light down to the surface, which undergoes the displacement. The second fiber collects the scattered, blocked, or reflected light. As the distance changes, the collection fiber transmits more or less light depending on the angle of entering rays of light with respect to the numerical aperture of the fiber. The numerical aperture (NA) of a fiber defines the angles over which light launched into it will successfully emerge at the other end. The NA of an optical fiber is defined as the sine of the angle defined by the fiber's mechanical axis and the maximum angle at which light is accepted and transmitted by the fiber.

All of the amplitude methods just described use a single source and a single detector. A two-fiber approach can be used to reduce signal corruption due to amplitude fluctuations, which will occur when using a single fiber. A second fiber placed along side the signal fiber, but not incorporating a path through the sensor, can serve as the reference fiber. Light from the source is launched into the two fibers with a beamsplitter or 3-db fiber coupler. It is assumed that the reference fiber will experience the same bending or other effects as the signal fiber. Two detectors are needed to resolve the signal, the usual technique being to divide the amplitude of the signal fiber by the amplitude of the reference fiber.

Light can be amplitude modulated a variety of other ways including spectrally selective absorbance, scattering, fluorescence, phosphorescence, and microbending. Of all the types of amplitude modulation, microbending is the most sensitive, approaching interferometric capability.

Microbending is an intrinsic amplitude modulation technique based on laterally induced strain in the fiber. The mechanism is based on the ejection of light from propagating core modes to cladding modes when a ray strikes that interface at less than the critical angle. The amplitude of light in a cladding mode decays exponentially with distance. The rays drop below the critical angle and transfer into the cladding. This is caused by the action of an external deforming device called a corrugator. The corrugator is a series of teeth or closely spaced, small-diameter wires that press directly on the fiber. The distance between the corrugations determines a spatial frequency. The sensitivity of the fiber to deformation is a function of this spatial frequency. The fiber is distorted in a serpentine fashion with small radii of curvature. Light leaks from a propagating mode to the cladding modes at these sharp bends. Davis [1985] reports that for deformations of < 1 micron, the intensity fluctuation will be proportional to deformation.

THEORY

The wave equation in circular cylindrical coordinates for a dielectric reduces to Helmholtz's equation in charge-free space and is

$$\Psi^2 E + (k^2 - \beta^2)E = 0$$

where $\beta = kn_f \sin\theta$, $k = 2\pi/\lambda$, θ is the zig-zag angle, and n_f is the core index for a wave propagating as $e^{\pm j\beta z}$. For guided modes $k^2 - \beta^2 > 0$ in the core, and ordinary Bessel functions result. When the variation of n is small compared to a wavelength of light, the wave equation is modified to:

$$\nabla^2 E + k^2[1 - 2\Delta(r/a)^2]E = 0$$

where r is radius of the ray, a is the radius of the core and $\Delta = [n^2(0) - n^2(a)]/2n^2(0)$, and is usually <<1. The solutions to the wave equation for an axially symmetric index are the orthogonal set of Hermite polynomials. The number of propagating modes in a right circular dielectric cylinder is shown to be [Ramo,1984]:

$$m = \beta a/\sqrt{(2\Delta)}$$

The theory of mode coupling in circular dielectric waveguides [Marcuse, 1974] shows that periodic axial distortions of a fiber couples light between adjacent modes. The solutions must be identical over one period. This coupling must satisfy

$$k - k' = 2\pi/\Lambda$$

where k and k' are longitudinal propagation constants, and Λ is the "mechanical" wavelength of the axial distortion.

Solving this equation in circular coordinates uses the WKB approximation from quantum mechanics. The mode separation coupling equation for a generic index profile is:

$$k_{m+1} - k_m = (a/(a+2))(2\sqrt{\Delta/a})(m/M)^{(a-2/a+2)}$$

where m and M are the mode order and number of modes, respectively, Δ is related to the index difference in the fiber, and a is a constant related to index profile. For step index fibers a is infinite, for parabolic index profiles it is equal to 2.

For a single-mode or parabolic index profile fiber all the modal groups are equally spaced in "k" space. Periodic distortions cause a linear outcoupling of guided modes to cladding or exponentially decaying modes. The theoretical mechanical wavelength for optimum outcoupling is:

$K = \sqrt{2\pi a/\Delta} = 2\pi a n_0/NA$, NA = fiber numerical aperture, n_0 is the on-axis index.

The above equation allows for the design of a practical microbend sensor. The elements of a sensor include an LED or laser diode, a step index delivery and collection fiber of high NA, the corrugator and sensor fiber of low NA, and a photodiode. Additional, critical components include a mode stripper

located before and after the corrugator, and a mode mixer. The mode stripping can be performed by wrapping the fiber around a mandrel of a few cm in diameter, or by coating the clad with a dark, absorbing paint. The stripper functions to remove cladding mode light and present to the corrugator section modes that are perfectly mixed and filled completely in k space. The mode mixer is placed after the light source and before the stripper, and insures that all modes in the fiber, of which there may be hundreds, are stimulated. The mode mixer itself is nothing mode than a corrugator which statically crimps a fiber. Located after the sense fiber is a fiber with a larger NA. The reason for this is to make the fiber sensor system insensitive to macrobending effects. The sense fiber is a low NA type to achieve maximum sensitivity. When connected to a high NA collection fiber, macrobending will only affect the high order modes. These higher modes are not populated because no propagating light exists in higher k space after having emerged from the sense fiber.

LEDs are much preferred for the light source due to their low noise. Laser diodes will yield a much higher minimum detectable displacement. Since the sensing will be done at essentially DC, it would be possible to use laser diodes if the detected signal was heavily filtered. Lasers are easier to optically couple to fibers than LEDs, but are a much more expensive solution for the light source.

A F/O microbend displacement sensor was reported [Lagakos, 1987] to have a 3%/micron sensitivity. It was fabricated with a 125 micron, graded index multimode fiber with an NA of 0.133. The corrugator had 18 teeth with a pitch of 3.2 mm. For very sensitive displacement sensors it is desired to have a small NA, large core diameter and large mechanical wavelength or pitch. But large core diameters result in mechanically stiff sensors which reduce sensitivity. There is a tradeoff between the two.

Also reported were much more enthusiastic performance numbers for sensor sensitivity in a different configuration. A piezoelectric transducer was used to sinusoidally squeeze the corrugator section with a driving amplitude of 10 Angstroms. Reported was a 24%/micron intensity variation, 8 times the sensitivity shown in a graph. The reason for the discrepancy was not explained. However, the LED offers Shot noise limited performance. The S/N ratio was 800.1 for a 10 Angstrom movement, for a minimum detectable movement of 0.01 Angstroms or 10^{-6} micron!

Polarization

Any amplitude F/O sensor must be relatively immune to signal loss in its fiber as it will be interpreted as a change in the quantity under measurement. The microbend sensor uses large NA fibers to aid in reducing this effect, but an assembled system of fibers, instrument package and natural forces (wind, footsteps, etc.) will always have a unpredictable effect on the level of the amplitude of the sensed quantity.

Fibers which are bent or kinked will cause mechanically induced birefringence, or different indices of refraction in two axes orthogonal to the fiber axis. A single-mode fiber for example, can extinguish half its propagating power if it exhibits the right amount of bending. There has been developed by fiber manufacturers a special type of fiber with large amounts of built-in birefringence. The reason is to dominate any environmentally caused strains in the fiber. If polarized light is launched into such a fiber,

it emerges polarized. These types of fiber are termed polarization maintaining (pm), polarization preserving (pp), or high birefringence (hi-bi) fibers.

A fiber sensor which analyzes the two states of polarization of the emerging light from a pm fiber has the potential to be much more robust than a simple amplitude sensor. Because the phase between the two states is the quantity measured it is not amplitude sensitive to macro or micro bending disturbances distributed along the fiber. This type of sensing also uses two sensors, but only one fiber. There can never be a question of whether fibers are experiencing the same environmental effects as in the case of the two fiber amplitude approach described earlier.

Birefringence is induced in bent single-mode fibers [Ulrich, 1980]. It is caused by compressive stress only in the radial direction in the plane of fiber curvature. A birefringent fiber which is bent produces a phase difference or optical retardation between the two principal axes of the fiber. One of these axes is called the fast axis, the other the slow axis. The intrinsic tensile stress of the manufactured fiber is cancelled by the bending-induced compressive stress. The retardation changes oppositely for the other principal axes of the fiber. Thus this technique produces a bipolar signal and potentially offers a sensitive way to measure displacements arising from tension or compression..

In a bent fiber the retardation Δ is:

$$\Delta = c(a/R)^2; \text{ in degrees/meter}$$

where c is -7.7×10^7 for fused silica, a is the fiber core radius and R is the radius of curvature. For N turns or loops of fiber the total retardation in degrees would be:

$$\beta = 2Npca^2/R$$

As an illustration, 1 turn of a 125-micron-diameter fiber bent into a loop of 2 cm diameter would have a total retardation of 180°.

In a bent birefringent fiber (pm) the induced stress partially cancels the intrinsic tensile stress. Because of the two axes of polarization within the fiber the retardation is changed according to:

$$\Delta = c(a/r)^2\cos 2\theta$$

where h is the azimuthal angle in the plane of bending as measured from the "slow" axis. Imai [1980] has conducted experiments and produced a F/O sensor based on bent pm fibers. It is noted from the previous equation that the retardation can have either sign depending on the axis of bending. It is posed that the total retardation in a completely general fiber system is a function both temperature and bending. By arranging the direction of bending of a two fiber system and how the signals are processed, one can make either a temperature insensitive bending sensor, or a bending insensitive temperature sensor. We obviously desire the former. Signal processing involves adding or subtracting the two signals from the photodetectors. Subtracting the two signals produces a response which is temperature insensitive and offers twice the sensitivity as a signal fiber.

A displacement sensor was produced [Imai, 1986] based on the bending of two coils of pm fiber. The coils were optically connected by 90°, and the sensed movement squeezed one coil while relaxing another. The cross coupling of the two coils made the pair of coils virtually temperature insensitive. One of the constraints of a polarization bend sensor is its characteristic sine-squared response. It is identical to the type of response one gets with using an optical strain polarimeter. If too much bending occurs the output signal is indistinguishable from that due to N*180° of phase shift, where N is the number of cycles that the output has cycled. Also, a sine-squared response has no sensitivity at 0 and 90°, and is usually optically biased to work at 45° of retardation. To recover the total phase over many N cycles it was proposed to use the strain induced loss curve of a bent fiber. This curve has a range of 30 db and allows for theoretically recovering any part of the polarmetric output. This is complicated to accomplish, and Imai did not accomplish it.

The reported sensitivity of the bent coupled coils was 360^0/mm about x = 0. If a useful phase is taken to be 45^0, a full-scale sensitivity of 125 micron is obtained. A 10 bit A/D would yield a minimum detectable resolution of 0.125 micron. One of the problems of this type of sensor is the accurate determination of the operating point on the sine-squared curve. The other problem is to constrain the sensor to operate over only one part of the curve. This is accomplished by design and proper installation and calibration techniques.

Interferometric (phase)

An interferometric F/O sensor is the most sensitive type. It is a two fiber approach that usually produces an intrinsically generated signal. Most classical interferometers can serve as F/O sensors, Michelson, Sagnac, Fabry-Perot, Twyman-Green and Mach-Zender. In the simplest case a section of fiber is bent. The resulting interference pattern is detected by a photodetector. Unfortunately, no sign is possible with these simple methods, and a heterodyne approach is taken. In this case the source is modulated by a high frequency, and the output is multiplied with the carrier frequency. The modulated output consists of sum and difference frequencies. Demodulation allows for the recovery of sign and magnitude.

Another way to produce strain in a fiber is to stretch it. An axially strained fiber undergoes compression in the radial direction. The difference between the axial and radial index of refraction depends on the fiber length, the so-called Pockels or photoelastic coefficients, and the radial strain. The total optical phase retardation in a strained fiber is:

$$\Delta\Phi = knL[1 - 0.25n^2(P_{12} - P_{11})]S_{11}$$

where k is the wavenumber of propagating light in the fiber, n is the core index, L is the total fiber length, the P's are Pockel's coefficients, and S_{11} is the axial strain. Strain-optic coupling coefficients of 10^{-9} radians/Pa have been reported [Davis, 1985] for F/O pressure transducers. A small transducer was built having a diameter of 0.3-mm and 20 mm long that was capable of detecting pressures down to 5.4 Pa. Virtually all interferometers are effective at measuring phase, and hence AC signals. Low frequency or DC noise sources such as 1/f and thermal noise limit the DC sensitivity of these interferometers. More

complexity, such as heterodyning can reduce or eliminate the problem at the price of complexity and expense.

Wavelength

Dichroic films can be applied to glass plates. This type of film has different absorption characteristics at different wavelengths. If the applied film is variable in spectral absorption over a small interval, an absolute type position measurement can be made.

Optical Triangulation

A lateral cell (position sensitive photodiode) can be used in conjunction with a mirror and fiber collimated beam to form a compact, sensitive absolute position detector. The minimum detectable movement in Angstroms over a range of 0.1 mm on the surface of the detector is:

$$\sqrt{(4 \times 10^{-8} \times \Delta f)/P},$$

where P is the incident power and Δf is the bandwidth of the detection process. If we assume 0.1 milliwatts and a bandwidth of 10 Hz, the minimum detectable position change is 6.3 Angstroms, or 6.3×10^{-4} microns. This is more than enough resolution than the 2.5×10^{-2} microns that the wall moves..

DISCUSSION

Both the microbend and bent coil technique deserve further investigation. While keenly aware of the desire to produce a possible commercial sensor based on the resulting technology, it should be pointed out that I am not aware of any commercial strain, pressure or displacement gauge which makes use of either microbend or polarization retardation means. In fact, there are only a few F/O based sensors that I know of. They are discussed below.

Metricor in Woodinville, WA, makes a pressure sensor based on a bowed diaphragm mounted onto the end of 125 micron fiber. I was involved in this work as a consultant in early 1983. This F/O sensor was for the medical field and only had a resolution of 0.5 mm Hg. They also produced a spectral (wavelength) modulated temperature sensor. A coating on the end of a fiber changes spectral characteristics as a function of temperature. It has 0.1°C resolution and a fast time constant of 0.02 seconds.

Laser Dynamics of Beaverton, OR, has a fiber sensor for measuring the cure of epoxy impregnated composites. The free radicals associated with curing change the index of the epoxy. In essence it functions similarly to a microbending fiber sensor.

APPENDIX REFERENCES

Davis, C.M., "Fiber optic sensors, an overview," *Optical Engineering*, Vol. 24, No. 2, pp. 347-351, 1985.

Imai, Y., and Ohtsuka, Y., "Compensated sensing based on retardation characteristics in a bent birefringent fiber," *J. Appl. Optics*, Vol. 25, No. 23, pp. 4444-4447, 1986.

Imai, Y., Rodrigues, M.A., Iizuka, K., "Temperature insensitive fiber coil for altimeters," *J. Appl. Optics*, Vol. 29, No. 7, 1990.

Lagakos, N., "Microbend fiber-optic sensor," *J. Appl. Optics*, Vol. 26, No. 11, pp. 2171-2180, 1987.

Marcuse, D., *Theory of Dielectric Optical Waveguides*, Academic Press, New York, 1974.

Ramo, S., et al., *Fields and Waves in Communications Electronics*, John Wiley and Sons, New York, 1984.

Ulrich, R., et al, "Bending induced birefringence in single mode fibers," *Opt. Letters*, 5, 273, 1980.